Photodissociation dynamics of the CH_2Cl radical: Ion imaging studies of the $Cl+CH_2$ channel

V. Dribinski, A. B. Potter, A. V. Demyanenko, and H. Reisler
Department of Chemistry, University of Southern California, Los Angeles, California 90089-0482

(Received 13 June 2001; accepted 16 July 2001)

The photodissociation of the chloromethyl radical, CH_2Cl, to chlorine atom and methylene is examined following excitation at selected wavelengths in the region 312–214 nm. CH_2Cl is produced in a molecular beam by using pulsed pyrolysis. Cl and CH_2 products are detected by laser ionization and their velocity and angular distributions are determined by using the ion imaging technique. The spectrum obtained by monitoring the Cl fragment yield as function of photolysis wavelength shows that throughout this wavelength region Cl atoms are major products. With 312–247 nm photolysis, the angular distributions are typical of a perpendicular transition ($\beta = -0.7$) and the main products are $CH_2(\tilde{X}\,^3B_1)+Cl(^2P_{3/2})$. The available energy is partitioned preferentially into the translational degrees of freedom. ''Hot band'' transitions are prominent in this region even in the molecular beam indicating that the geometries of the ground and excited states of CH_2Cl must be very different. With 240–214 nm photolysis, the angular distributions are typical of a parallel transition ($\beta \sim 1.2$), and the predominant products are $Cl(^2P_{3/2})$ and $Cl(^2P_{1/2})$, with $CH_2(\tilde{a}\,^1A_1)$ as the main cofragment. A large fraction of the available energy is partitioned into internal energy of $CH_2(\tilde{a}\,^1A_1)$. Comparison with the *ab initio* calculations of Levchenko and Krylov presented in the accompanying paper enables the assignment of the perpendicular and parallel transitions predominantly to $1\,^2A_1 \leftarrow 1\,^2B_1$ and $2\,^2B_1 \leftarrow 1\,^2B_1$ excitations, respectively, and both upper states are probably repulsive in the C–Cl coordinate. The electronic states of the products obtained via these two transitions are in agreement with the predictions of a simple diabatic state correlation diagram based on the calculated vertical energies of the upper states. © *2001 American Institute of Physics.* [DOI: 10.1063/1.1400130]

I. INTRODUCTION

The photoinitiated chemistry of free radicals is of great importance in atmospheric and environmental chemistry,[1] but its study is hindered by experimental and theoretical difficulties. Halogenated methyl radicals are important in stratospheric chemistry, since they can provide an additional source of photolytic halogen atoms, but their absorption spectra in regions where the actinic flux is high are still unknown. Molecules and radicals with halogen substituents often possess low-lying valence states associated with the promotion of an electron from a lone pair centered on the halogen to an antibonding orbital, thereby weakening the carbon-halogen bond. In addition, radicals usually have low ionization potentials, and therefore they have Rydberg states that lie in the same energy region as their lowest valence states. Because Rydberg states are often correlated with excited electronic states of the products, the interactions between the Rydberg and valence states and their dependence on internuclear distances are of crucial importance to the dynamics.[2] An intriguing aspect concerning the low-lying Rydberg states is the extent of their penetration into the core region. For example, if the nodes in the radial Rydberg wave function lend a significant antibonding character to regions of the wave function associated with specific bonds, this penetration will influence the photodissociation dynamics. Radicals often dissociate to more stable species, and therefore many of their excited states are dissociative or predissociative, giving rise to multiple dissociation pathways.

As shown by Levchenko and Krylov in the accompanying paper,[3] determining the relative order of Rydberg and valence excited states of CH_2X radicals and the associated electronic transition dipole moments requires high level of theory. The energies of the excited states depend sensitively on such factors as how strongly the halogen lone pair is bound, the energetics and nature of the relevant molecular orbitals, and the Franck–Condon factors for absorption.

In this paper we describe the first experimental results on the photodissociation of the chloromethyl radical, CH_2Cl, which can serve as a prototype for halogenated methyl radicals. CH_2Cl is produced as a primary product in the pyrolysis and photolysis of CH_2ClX molecules, where X is a halogen, and in the reaction of Cl or F with CH_3Cl.[4] To date the only reported electronic absorption is a strong, unstructured band centered at ~200 nm (where the cross section is $1.45 \times 10^{-17}\,cm^2$), which extends to ~220 nm.[4] No absorption measurements at wavelengths longer than 220 nm have been reported, although the existence of an excited electronic state around 5 eV has been suggested based on analysis of microwave spectra;[5] i.e., an absorption band at ~250 nm.

The photochemistry of CH_2Cl is interesting from another perspective. The radical has several dissociation channels with very similar thermochemical thresholds:[6–13]

$$CH_2Cl \rightarrow Cl + CH_2, \quad \Delta H = 391 \pm 5 \text{ kJ mol}^{-1},$$
$$H + CHCl, \quad \Delta H = 395 \pm 5 \text{ kJ mol}^{-1},$$
$$H_2 + CCl, \quad \Delta H = 382 \pm 5 \text{ kJ mol}^{-1},$$
$$HCl + CH, \quad \Delta H = 384 \pm 5 \text{ kJ mol}^{-1}.$$

The main uncertainties in calculating the enthalpy changes in the decomposition derive from the heat of formation of the CH_2Cl radical.[8–13] Thus, the *relative* dissociation thresholds are known to a better accuracy ($\sim \pm 2$ kJ mole^{-1}). The first two channels involve simple bond-fission reactions ending in two free radicals, and on the ground electronic state they are likely to evolve without significant barriers. Because their thresholds are so similar, the branching ratio between them is important. The last two channels are expected to have significant activation barriers. In this paper we report results solely on the $Cl + CH_2$ channel.

In our experiments, we use pulsed pyrolysis to prepare the radicals in a molecular beam, and the ion imaging technique for photofragment detection. We clearly identify two distinct electronic transitions in the region 312–214 nm, and based on the *ab initio* results[3] we assign their upper states as $1\,^2A_1$ and $2\,^2B_1$. Both are dissociative, and give rise to Cl atom as a major product. We argue that the geometries of the ground $1\,^2B_1$ state and the first excited $1\,^2A_1$ state must be substantially different, as evidenced by strong ''hot band'' absorption. We also comment on the electronic states of the CH_2 cofragment and the spin–orbit state populations of the Cl atoms. We end by discussing a state correlation diagram relevant to the dissociation to $Cl + CH_2$, and the possible participation of the $2\,^2A_1$ Rydberg state.

II. EXPERIMENTAL METHODS

A. Radical production

CH_2Cl radicals are produced by thermal decomposition of chloroiodomethane (CH_2ClI) in a pulsed pyrolysis source. The choice of the precursor is dictated by the energetics of dissociation of CH_2ClI on the ground electronic state. According to the known thermochemical data,[6–13] the lowest dissociation channel is $CH_2Cl + I$ ($\Delta H^\circ = 242$ kJ/mol). The next channel, $CHCl + HI$, has $\Delta H^\circ = 337$ kJ/mol, but is expected to have a significant activation barrier, while the third channel is $CH_2I + Cl$ ($\Delta H^\circ = 367$ kJ/mol). Therefore, it should be possible to optimize the conditions in the pulsed pyrolysis source to maximize production of CH_2Cl.

The experiments are performed using a pulsed molecular beam (0.5–1.0% CH_2ClI seeded in 2.0 atm of He or Ar). The gas mixture is prepared by passing the carrier gas over CH_2ClI (Fluka, $\geqslant$97% purity) kept at $-29\,^\circ$C (*o*-xylene slush) or $0\,^\circ$C (ice). This mixture is expanded through a pulsed piezoelectric valve (10 Hz repetition rate) with an attached SiC tube nozzle (1 mm i.d.), and our design is similar to that of Chen and co-workers.[14] The nozzle has a 1-cm long resistively heated zone.

In our experiments, the SiC tube nozzle is heated to a temperature of $\sim$1800 K which results in removal of I atoms from CH_2ClI with an efficiency of more than 50%. The temperature of the nozzle was estimated from a voltage/temperature calibration curve obtained in a separate experiment by using an optical pyrometer. The pyrolysis efficiency is estimated by comparing the REMPI signals of iodine fragments obtained by photodissociation of the CH_2ClI precursor in the molecular beam with the heating of the pyrolysis tube turned on and off. As the temperature of the nozzle is increased, the I atom signal from the photodissociation of CH_2ClI diminishes. However, above a certain temperature, the efficiency of production of CH_2Cl starts to decrease as a result of both its thermal decomposition, and the increasing contribution of higher-threshold dissociation pathways in CH_2ClI. For example, fragments such as Cl atoms and HI are produced in the pyrolysis source. Under our experimental conditions, a large depletion (more than a factor of 2) of the iodine photofragment signal is observed, while at the same time the amount of thermal Cl atoms does not exceed 1% of the total Cl signal.

After the supersonic expansion, the radicals are skimmed twice and introduced into the reaction chamber. In order to minimize background signals from the photodissociation of CH_2ClI, the experiments are carried out at the leading edge of the molecular pulse exiting the nozzle. With He as the carrier gas, the heavy, iodine-containing species arrive at the reaction chamber delayed by approximately 30 μs with respect to the light species, as a result of velocity slip.[15] Thus, the leading edge of the molecular pulse does not contain a significant amount of CH_2ClI. When Ar is used as a carrier gas, there is no velocity slip, and substantial background subtraction of signals from the photodissociation of the precursor is necessary, degrading the signal to noise ratio in the experiment.

B. Photodissociation and detection of products

The dissociation of CH_2Cl is examined at selected wavelengths in the region 311.8–214 nm. Radical photolysis and product detection are achieved by using the frequency-doubled output of a Nd:YAG or excimer-laser pumped dye laser systems. One system is used for photolysis (pump) and the other to probe the products. The pump and probe lasers are both linearly polarized, and introduced coaxially at a right angle to the molecular beam. The polarizations of the two lasers are fixed parallel to each other and kept perpendicular to the plane defined by the molecular beam and the laser propagation axis. The time delay between the pump and probe lasers is kept at 0–5 ns.

Velocity map imaging combined with resonance enhanced multiphoton ionization (REMPI) is used for product detection. Our ion-imaging arrangement has been described in detail elsewhere.[16,17] In brief, it consists of an ion-acceleration stage, a 60-cm long drift tube, and a CCD camera that monitors a phosphor screen coupled to a MCP detector. The ion-optics consists of a repeller, an open extractor electrode (50 mm hole), and an open ground electrode (25 mm hole). At an optimal voltage ratio of the repeller and extractor plates, all ions with the same initial velocity are focused onto the same spot on the MCP detector.

We use $2+1$ REMPI to detect $Cl(^2P_{3/2})$ ($\lambda = 235.337$ nm) and $Cl(^2P_{1/2})$ ($\lambda = 235.205$ nm).[18] Other Cl-atom detection wavelengths in the region 235–240 nm have

smaller intensities and are only used for calibration purposes. Due to the Doppler width of the Cl absorption band, the probe frequency is scanned over the entire bandwidth to ensure that the images include all product velocities.

$CH_2(\tilde{X}\,^3B_1)$ radicals are monitored by $2+1$ REMPI at $\lambda = 311.80$ nm, as proposed by Hudgens and co-workers.[19] Although the REMPI spectrum has not been assigned, it shows clear structures with the largest peak at 311.80 nm, and the intermediate state is assigned as a Rydberg $3p$ state.[19] No REMPI scheme for the detection of $CH_2(\tilde{a}\,^1A_1)$ is known, and no REMPI signal from CH_2Cl could be detected, because of the rapid dissociation of the radical in the wavelength region studied here. A weak REMPI signal is observed at 302–318 nm, which is a result of two-photon excitation, probably to a Rydberg state.

C. Data analysis

Two types of background signals are subtracted from the images obtained in two-color pump and probe experiments: (i) the signal obtained from the molecular beam pulse, but with the pump laser off accounts for background generated by the probe laser alone; (ii) the signal obtained with both pump and probe lasers off accounts for the ''dark noise'' of the CCD camera. In addition the signals obtained with the pyrolysis tube heating turned on and off are always compared.

The resultant images are normalized to the relative sensitivity of the pixels in the CCD camera and deconvoluted from the response function of the data acquisition system. The inverse Abel transform is performed on the normalized signal to extract the 3D distributions that give rise to the 2D projections.[16,17,20]

III. RESULTS AND ANALYSIS

Two electronic transitions are clearly identified in our experiments. In the region 311.8–247 nm, $CH_2(\tilde{X}\,^3B_1)$ and $Cl(^2P_{3/2,1/2})$ products derive from dissociation via a perpendicular electronic transition in CH_2Cl. At wavelengths shorter than about 240 nm the $Cl(^2P_{j=3/2,1/2})$ products exhibit angular distributions that are characteristic of a parallel transition.

Figure 1 depicts typical Abel transformed images of $Cl(^2P_{3/2})$ and $CH_2(\tilde{X}\,^3B_1)$ obtained with 266 nm photolysis. In this figure, as in all other images, the electric field vector of the photolysis laser is parallel to the vertical direction of the image plane. Both images have an angular distribution characteristic of a perpendicular transition. The effective recoil anisotropy parameter β is -0.7 ± 0.1. Analysis of the velocities shows that the Cl and CH_2 fragments match by linear momentum.

Figures 2 and 3 show the total photoproduct center-of-mass (c.m.) translational energy distributions obtained by monitoring $Cl(^2P_{3/2})$ and $CH_2(\tilde{X}\,^3B_1)$ at dissociation wavelengths 280, 266, and 247 nm. These distributions are derived from the speed distributions of each fragment. The speed distributions of $Cl(^2P_{3/2})$ and $CH_2(\tilde{X}\,^3B_1)$ are first obtained from the transformed images by integrating the signal

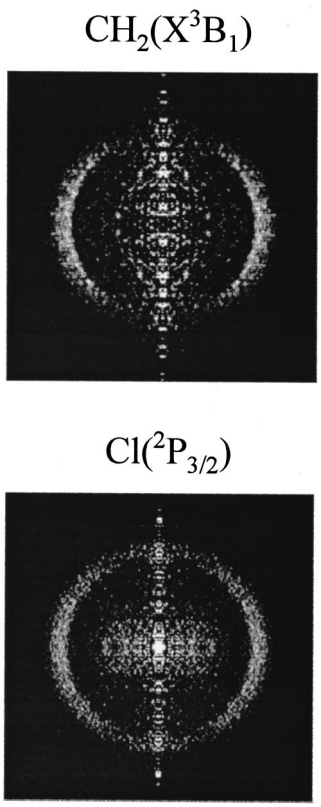

FIG. 1. Abel transformed images of $CH_2(\tilde{X}\,^3B_1)$ (top) and $Cl(^2P_{3/2})$ (bottom) obtained from CH_2Cl photodissociation at 266 nm. $CH_2(\tilde{X}\,^3B_1)$ and $Cl(^2P_{3/2})$ were detected by $(2+1)$ REMPI at 311.8 nm and 235.34 nm, respectively. The size of each image is adjusted to fill the detector plane. The electric field vector of the photolysis laser is parallel to the vertical direction of the image plane.

for each radial distance from the center (after calibrating each image for conversion from distance to speed). Each speed distribution is then converted to the translational energy distribution of the specific fragment, and the total c.m. translational energy distribution, E_t, is finally derived by scaling according to the mass ratio dictated by momentum and energy conservation. For $Cl(^2P_{3/2})$ atoms, the E_t distribution can be directly converted to internal energy distribution of the matching CH_2 fragment. The situation is more complicated for the $CH_2(\tilde{X}\,^3B_1)$ product, since neither a single rovibrational state nor the total state population is monitored (see below). Small signals from $Cl(^2P_{1/2})$, which is 881 cm^{-1} higher in energy than ground state $Cl(^2P_{3/2})$,[18] are also observed at all wavelengths, and their associated energy distributions are similar to those of $Cl(^2P_{3/2})$.

The widths of the translational energy distributions for Cl correspond to a range of internal excitations in the CH_2 co-fragment. Note in particular the two major peaks in this distribution, which are approximately 3000 cm^{-1} apart, and may correspond to the ground $\tilde{X}\,^3B_1$ and the first excited $\tilde{a}\,^1A_1$ ($T_e = 3147\ cm^{-1}$)[7] states of CH_2. In Figs. 2 and 3, arrows indicate the maximum allowed translational energy of the products, E_t^{max}, calculated for photolysis of CH_2Cl in its *ground* vibrational state:

$$E_t^{max} = h\nu - D_0. \tag{1}$$

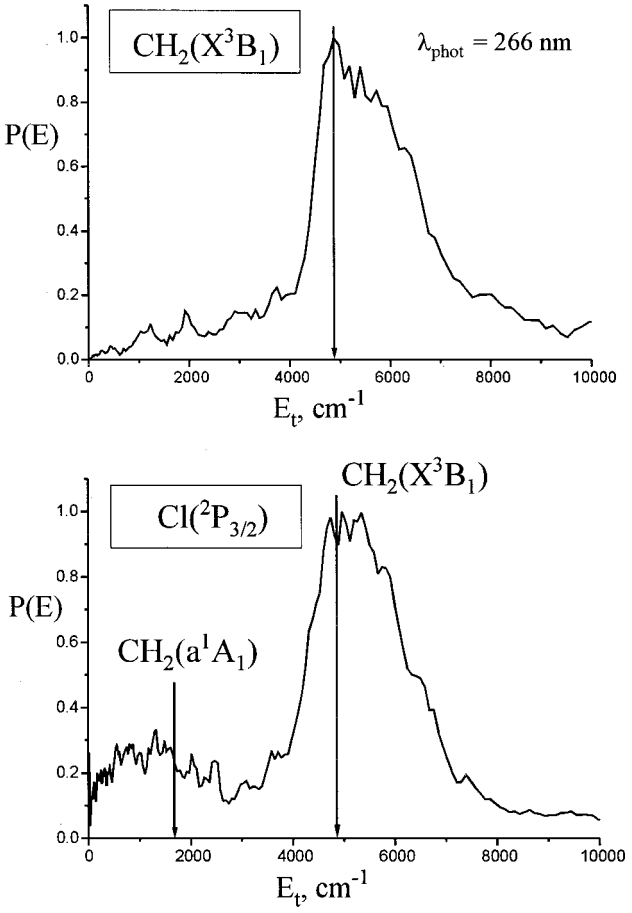

FIG. 2. $CH_2(\tilde{X}\,^3B_1)$ (top panel) and $Cl(^2P_{3/2})$ (bottom panel) signals obtained following 266 nm dissociation of CH_2Cl (37 594 cm^{-1}) plotted as a function of the total c.m. photofragment translational energy, E_t. The details of the transformation of the Abel transformed images to total c.m. translational distributions are given in the text. The long arrows show the energy threshold calculated using $D_0 = 391$ kJ/mol. The short arrow in the Cl energy distribution shows the energy threshold for production of $CH_2(\tilde{a}\,^1A_1)$.

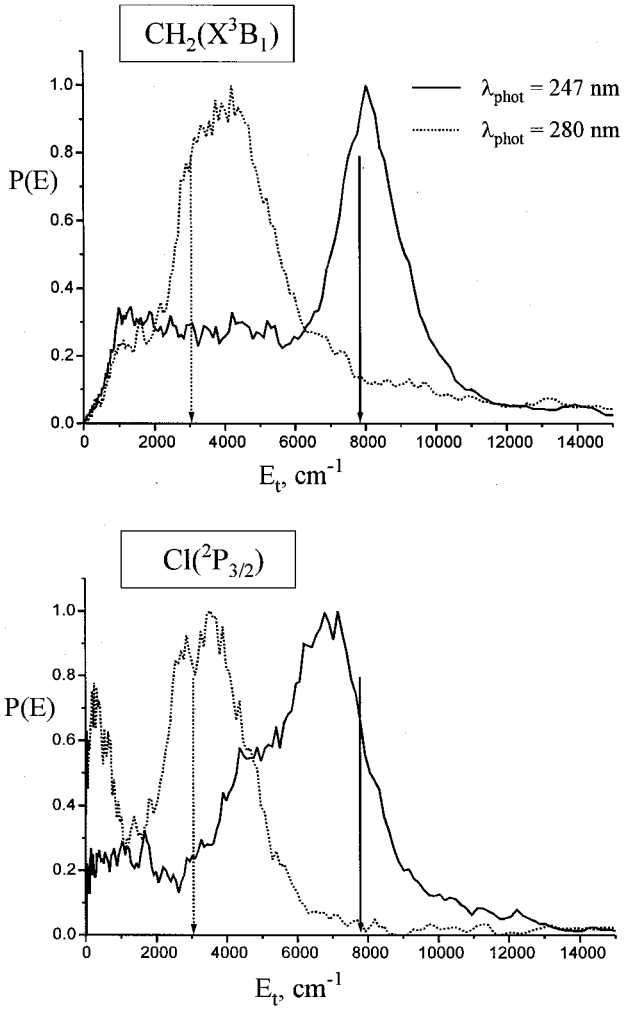

FIG. 3. $CH_2(\tilde{X}\,^3B_1)$ (top panel) and $Cl(^2P_{3/2})$ (bottom panel) signals obtained following 247 nm (40 486 cm^{-1}; solid lines) and 280 nm (35 714 cm^{-1}; dotted lines) dissociation of CH_2Cl plotted as a function of the total c.m. photofragment translational energy, E_t, as described in Fig. 2. The arrows indicate the energy thresholds calculated using $D_0 = 391$ kJ/mol.

The complete energy balance for CH_2Cl dissociation is given by

$$E_{\text{int}}(CH_2Cl) + h\upsilon = D_0 + E_t + E_{\text{int}}(CH_2) + E_{\text{int}}(Cl), \qquad (2)$$

where $h\upsilon$ is the photon energy, D_0 is the dissociation threshold of the CH_2Cl radical, and $E_{\text{int}}(CH_2Cl)$, $E_{\text{int}}(CH_2)$, and $E_{\text{int}}(Cl)$ are the internal energies (rotational, vibrational, and electronic) of the respective reactant and fragments. The value of D_0 was derived from the enthalpies of formation of CH_2Cl, CH_2, and Cl to be 391 ± 5 kJ/mol ($32\,690 \pm 420$ cm^{-1}).[6–13] As seen from Figs. 2 and 3, large fractions of the products have translational energies exceeding $E_t^{\max}$.

Products with excess translational energy can arise from the dissociation of vibrationally "hot" CH_2Cl radicals [i.e., $E_{\text{int}}(CH_2Cl) \neq 0$]. The experiments described above were performed using He as a carrier gas. Based on previous work,[21,22] effective rotational cooling of CH_2Cl radicals is expected in the pyrolysis source, but He is not efficient in relaxing the vibrational excitations. Thus, the high energy tails of the observed product distributions are attributed mainly to the dissociation of vibrationally excited ("hot") CH_2Cl radicals. A similar behavior is observed at other wavelengths in the range 312–247 nm. Another possible source of fragments with excess kinetic energy is two-photon dissociation of CH_2Cl. However, the products of such dissociation (i) should have considerably larger translational energies since absorption of a second photon at these wavelengths would impart additional energy of more than 30 000 cm^{-1}, and (ii) must show higher power dependence on pump laser energy. Neither was observed in our experiments, and this rules out the presence of signal from two-photon dissociation.

In order to confirm that products with excess kinetic energy result from dissociation of vibrationally excited radicals, we carried out experiments with Ar as a carrier gas. Figure 4 shows an image of $Cl(^2P_{3/2})$ obtained from the dissociation of CH_2Cl at 266 nm in Ar carrier gas and detected at 235.34 nm, and Fig. 5 shows the corresponding c.m. translational energy distribution. Similar results were obtained at 247 nm. Compared with the He experiments, two main differences are observed. First, the translational energy distribution becomes narrower with the largest peak at high

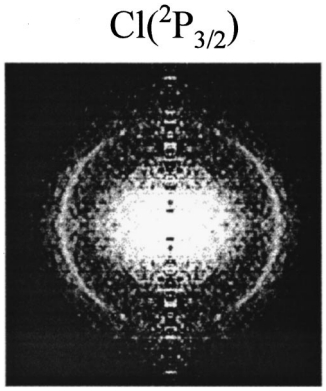

FIG. 4. Abel transformed image of $Cl(^2P_{3/2})$ obtained from CH_2Cl photodissociation at 266 nm using Ar as a carrier gas. $Cl(^2P_{3/2})$ was detected by (2+1) REMPI at 235.34 nm. The electric field vector of the photolysis laser is parallel to the vertical direction of the image plane.

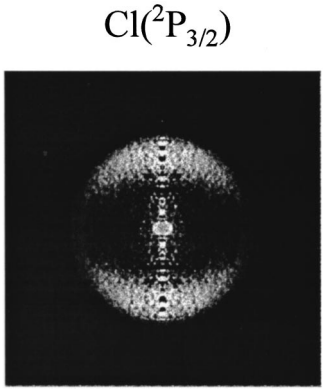

FIG. 6. Abel transformed image of $Cl(^2P_{3/2})$ obtained from CH_2Cl photodissociation at 235.34 nm in a one-color experiment. The electric field vector of the photolysis laser is parallel to the vertical direction of the image plane.

energies corresponding to the dissociation of vibrationally cold CH_2Cl. The short arrows in Fig. 5 indicate the energy thresholds of steps that are discernible in the Cl energy distribution obtained in the Ar carrier. These steps are separated by $\sim$800 cm^{-1}, which is the frequency of the C–Cl stretch in CH_2Cl. Second, the relative intensity of the low energy peak [which is likely to contain $CH_2(\tilde{a}\,^1A_1)$] is larger. In the experiments with Ar, we were unable to detect $CH_2(\tilde{X}\,^3B_1)$ by REMPI. This may be a result of the much smaller signal levels obtained in general when using Ar as a carrier gas in the pyrolysis source, and/or the smaller fraction of $CH_2(\tilde{X}\,^3B_1)$ relative to $CH_2(\tilde{a}\,^1A_1)$ produced in the dissociation of ground state CH_2Cl. We cannot rule out, however, the possibility that the REMPI signals that correspond to Cl atoms with the lowest translational energies derive also from other sources, since we do not have direct diagnostics for $CH_2(\tilde{a}\,^1A_1)$. We attempted to improve the vibrational relaxation in CH_2Cl by using a carrier gas that is 1:7 CF_4:He. The results, however, were similar to those obtained with Ar as the carrier gas.

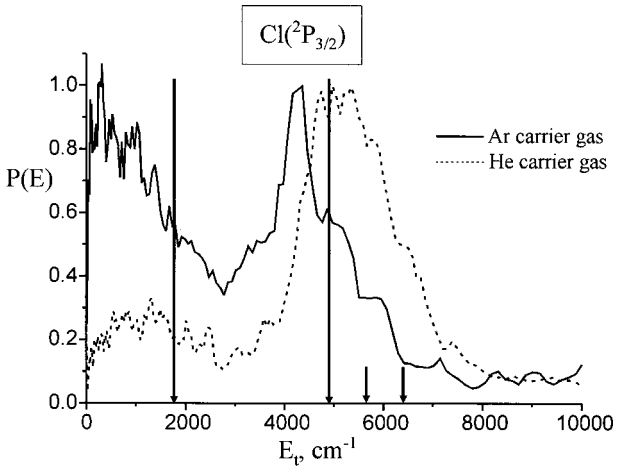

FIG. 5. $Cl(^2P_{3/2})$ signals obtained following 266 nm dissociation of CH_2Cl (37 594 cm^{-1}) using Ar (solid line) or He (dotted line) carrier gas plotted as a function of the total c.m. photofragment translational energy, E_t. The long arrows indicate the energy thresholds for the production of $CH_2(\tilde{X}\,^3B_1)$ and $CH_2(\tilde{a}\,^1A_1)$ from vibrationally "cold" CH_2Cl (see Fig. 2). The short arrows show the positions of "hot band" peaks which are resolved in the Ar experiments.

The widths of the energy distributions of the CH_2 fragments in Figs. 2 and 3 require comment. Each CH_2 fragment can correlate with either $Cl(^2P_{3/2})$ or $Cl(^2P_{1/2})$ and, therefore, the translational energy distribution for each particular $CH_2(\nu,J)$ should consist of two narrow peaks 881 cm^{-1} apart, though in the present case the peak correlated with $Cl(^2P_{1/2})$ would be small. As seen in Figs. 2 and 3, the translational energy distributions of CH_2 obtained in our experiments are much broader than the experimental resolution ($\Delta E/E \sim 0.04$). This is especially clear in the 247 nm distribution, which has a smaller "hot band" component. A possible cause for such broad distributions is the simultaneous detection of multiple rotational levels of CH_2 encompassed in the bandhead at 311.8 nm. This conclusion is supported by calculations of the approximate positions of the rotational lines of the 0–0 vibronic band of the CH_2 electronic transition (Appendix). The rotational constants for the ground electronic state of CH_2 are very close to those of the $3p$ Rydberg state (the intermediate state in the 2+1 REMPI detection scheme),[19] and therefore several rotational transitions have almost the same energy. As shown in the Appendix, for the ^QQ rotational branch ($\Delta N=0$, $\Delta K=0$), transitions involving rotational levels up to $N=6$, $K=5$ have transition energies that differ by less than 10 cm^{-1}. Because the upper electronic state is broadened by intramolecular interactions,[19] many of these levels are detected simultaneously. At the same time, the rotational energies of these levels can cover a range of up to 2000 cm^{-1}, and thus the resulting translational energy distributions of the detected CH_2 products can be broad.

When the dissociation wavelength is tuned to the region 240–214 nm, the angular distributions of the products change qualitatively. Shown in Fig. 6 is an image of $Cl(^2P_{3/2})$ obtained in a one-color experiment at 235.34 nm. The angular distribution of $Cl(^2P_{3/2})$ is typical of a parallel electronic transition in CH_2Cl, as are all the other distributions of $Cl(^2P_{3/2,1/2})$ in the 240–214 nm photolysis region.

Figure 7 shows the c.m. translational energy and the an-

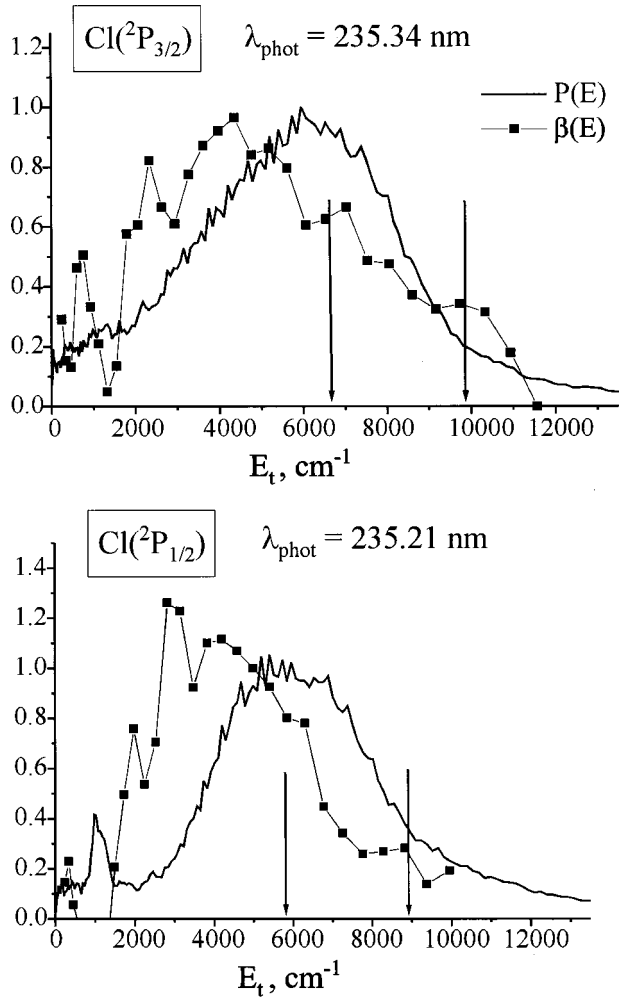

FIG. 7. Total c.m. translational energy (solid lines) and angular anisotropy parameter (squares) distributions of $Cl(^2P_{3/2})$ (upper panel) and $Cl(^2P_{1/2})$ (lower panel) obtained in one-color experiments at 235.34 nm and 235.21 nm, respectively. Arrows show the energy thresholds for production of $CH_2(\tilde{X}\,^3B_1)$ and $CH_2(\tilde{a}\,^1A_1)$.

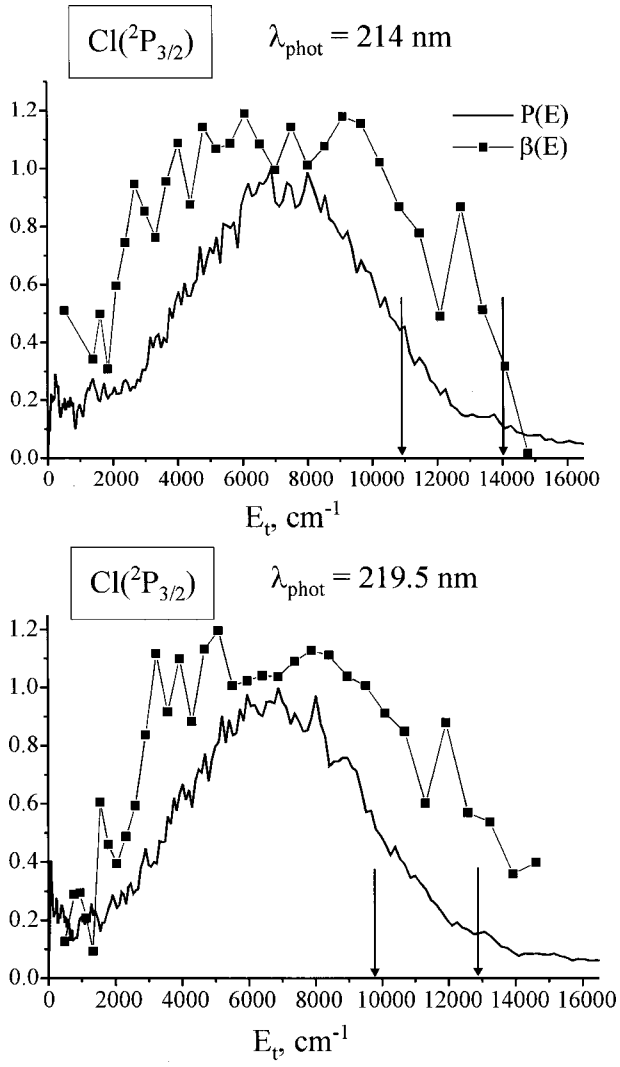

FIG. 8. Total c.m. translational energy (solid lines) and angular anisotropy parameter (squares) distributions of $Cl(^2P_{3/2})$ obtained from the dissociation of CH_2Cl at 214 nm (upper panel) and 219.5 nm (lower panel) and detected by (2+1) REMPI at 235.34 nm. Arrows show the energy thresholds for production of $CH_2(\tilde{X}\,^3B_1)$ and $CH_2(\tilde{a}\,^1A_1)$.

isotropy parameter distributions obtained by monitoring $Cl(^2P_{3/2})$ and $Cl(^2P_{1/2})$ in one-color experiments at 235.34 nm and 235.21 nm, respectively. For a fast, parallel transition in CH_2Cl, the maximum anisotropy parameter $\beta=2$ will be obtained when the transition dipole moment is parallel to the C–Cl bond. However, in both $Cl(^2P_{3/2})$ and $Cl(^2P_{1/2})$, β is considerably smaller than 2, and in addition it is speed dependent, i.e., products with higher translational energies have smaller values of β than those with lower translational energies. At 219.5 and 214 nm, however, β is characteristic of a parallel transition at all speeds where the Cl population is significant ($E_t > 2000\,\mathrm{cm}^{-1}$) as seen in Fig. 8. We note that the speed and β distributions are the least reliable at energies below $\sim 2000\ \mathrm{cm}^{-1}$ for the following reasons: (i) Errors from the Abel transformation accumulate in the low velocity region of the image (see, for example, Fig. 6); (ii) the product signal at low E_t is quite low; (iii) a small, unknown contamination sometimes gives rise to a narrow feature with negative β in the region 1500–2000 cm^{-1}. The error bars on the measured values of β at $E_t > 2000\,\mathrm{cm}^{-1}$ are typically ± 0.1. We conclude that the observed spectrum at 240–235 nm is a combination of excitations via parallel and perpendicular transitions, each giving rise to Cl product with a different translational energy distribution. The fraction of the parallel component increases gradually as the wavelength is decreased from 240 nm to 214 nm.

In Figs. 7 and 8 we also mark the energy thresholds for the production of the ground and first excited states of CH_2. Very little Cl is observed that corresponds to $CH_2(\tilde{X}\,^3B_1)$. This, along with the fact that we are unable to detect $CH_2(\tilde{X}\,^3B_1)$ by REMPI at these wavelengths even though the Cl signal is quite strong, indicates that in excitation via the parallel transition, $CH_2(\tilde{a}\,^1A_1)$ is probably the major product.

We note that at 214 and 219.5 nm, there are only few fragments with translational energies exceeding significantly $E_t^{\max}$, and no change is observed when the He carrier gas is replaced by Ar. Hence, we conclude that the parallel transi-

tion is not as severely affected by ''hot band'' excitation as is the perpendicular transition.

IV. DISCUSSION

A. Identification of the radical precursor

Since the results reported here are based exclusively on monitoring photofragments, it is essential to verify, before attempting an interpretation, that the precursor of all the observed products is CH_2Cl. The absence of a REMPI peak of molecular CH_2Cl in this wavelength region is attributed to the fast dissociation ($\beta=-0.7$ and 1.2 for the perpendicular and parallel transitions, respectively). We note, however, that weak $2+1$ REMPI peaks corresponding to CH_2Cl cations are observed upon excitation at ~376 and 302–318 nm,[23] and are attributed to two photon excitations to Rydberg states.[3,24]

For the products observed via the perpendicular transition (312–247 nm), the identification of CH_2Cl as the precursor is based on several observations. First, both $CH_2(\tilde{X}\,^3B_1)$ and $Cl(^2P_{3/2})$ photofragments are detected under the same experimental conditions (He carrier gas), exhibiting identical angular distributions and the same maximum value of linear momentum.

Second, no other significant sources of the CH_2 and Cl pair are expected to be present in the leading region of the molecular pulse. As mentioned above, parent CH_2ClI molecules are largely absent because of velocity slip. The thermochemistry of CH_2ClI dictates that CH_2I and CHCl would be only minor pyrolysis products under our experimental conditions, and they would lead to Cl and CH_2 products that are not momentum matched.

Last, although only a small signal from ground state CH_2 is detected in the experiments with Ar carrier gas, the $Cl(^2P_{3/2})$ fragments exhibit a similar structure in their energy distributions to that obtained with He carrier gas; i.e., two broad peaks separated by about 3000 cm^{-1}, which corresponds to the energy separation of the $\tilde{X}\,^3B_1$ and $\tilde{a}\,^1A_1$ states of CH_2. In Ar, the translational energy associated with most of the Cl products is smaller than the maximum calculated for dissociation of vibrationally ''cold'' CH_2Cl (see below). In addition, the same angular anisotropy parameter is obtained for Cl produced with He and Ar carrier gases.

Likewise, we believe that CH_2Cl is the main precursor of the $Cl(^2P_{3/2,1/2})$ products from the parallel transition at 240–214 nm. The energy distributions of the Cl fragments can be well fit by assuming that the precursor is ground state CH_2Cl, and that a large fraction of the Cl atoms are associated with singlet $CH_2(\tilde{a}\,^1A_1)$ cofragments (Figs. 7 and 8). The angular distributions of the Cl atoms change gradually as the dissociation wavelength decreases from 247 nm, where a perpendicular transition is observed, to shorter wavelengths. In the region 240–235 nm the value of β is speed dependent, ranging from ~0 at high Cl speeds to 1.2 at low speeds, suggesting contributions from both parallel and perpendicular transitions. At 219.5 and 214 nm, the parallel transition dominates, and the β parameter is largely speed independent for $E_t > 2000\,cm^{-1}$.

The experiments in the 240–214 nm photolysis region were performed under the same pyrolysis conditions as those at 312–247 nm, and therefore we do not expect that sources other than CH_2Cl would contribute significantly to the Cl or CH_2 signals. We conclude that Cl products with positive and negative values of β result from dissociation following parallel and perpendicular transitions, respectively, in CH_2Cl.

B. Electronic transitions in CH_2Cl

1. Perpendicular transition

Analysis of the Cl and CH_2 angular distributions indicates that in the region between 311.8 nm (3.98 eV) and 247 nm (5.02 eV) the excited electronic state(s) of the CH_2Cl radical is (are) accessed via a perpendicular transition. At all wavelengths in this region, the angular distributions of both CH_2 and Cl products can be fitted with a negative recoil anisotropy parameter, $\beta=-0.7\pm0.1$. This implies fast, direct dissociation on a repulsive region of the potential energy surface. As established previously,[3,5,25–27] CH_2Cl is planar in its ground state and has C_{2v} symmetry. Since the ground state is of B_1 symmetry, the presence of a perpendicular transition indicates excitation to either A_2 or A_1 electronic states, whose transition dipole moments lie either in-plane or out-of-plane, respectively, but perpendicular to the Cl recoil direction.

Figures 2, 3, and 5 show clearly that with He carrier gas, dissociation of vibrationally excited CH_2Cl contributes significantly to the observed CH_2 and Cl signals, especially at wavelengths longer than 260 nm. The fraction of fragments with translational energies greater than E_t^{max} is much larger than expected had the vibrationally excited radicals in the molecular beam been excited with the same efficiency as the unexcited radicals. The absorption spectrum can only be rationalized by postulating a very large increase in the Franck–Condon factors for ''hot band'' excitation due to the vibrational motions in the radical. Therefore, we argue that the ground and excited electronic state geometries must be rather different. Note that even in Ar some of the Cl fragments have energies exceeding E_t^{max}. This energy distribution is structured, with the bands separated by the C–Cl stretch energy in CH_2Cl. Apparently, this mode is not cooled efficiently even in Ar or CF_4:He. We conclude that the ground and electronically excited states of CH_2Cl must have quite different C–Cl bond lengths. The strong propensity to ''hot band'' excitation suggests also that the excited state may be bound in the C–Cl coordinate, with excitation accessing mainly the repulsive wall. ''Hot bands'' resulting from excitation of other vibrational modes, such as the out-of-plane bend (~390 cm^{-1}), cannot be excluded.[25,26]

The definitive assignment of the symmetry of the excited state is obtained from the *ab initio* calculations of Levchenko and Krylov.[3] Using the EOM–CCSD method[28] with 6-311(3+,3+)G(3df,3pd) basis set, they have assigned the lowest excited states of CH_2Cl, and calculated their vertical excitation energies and electronic transition moments (see Table II in Ref. 3).[29] The first allowed transition is to the $1\,^2A_1$ state, and there are no low-lying states of $^2A_2$ symmetry. The calculated value of the vertical excitation energy for

the $1\,^2A_1$ state is 4.92 eV, which corresponds to an excitation wavelength of 252 nm. This is where we expect the maximum in the absorption cross section, as well as the largest product yield originating in vibrationally unexcited radicals. This is confirmed by the results shown in Figs. 2 and 3. While at wavelengths $\geqslant$280 nm most of the CH_2 and Cl signals are attributed to ''hot band'' excitation, at 266 nm the contribution of fragments with translational energies exceeding $E_t^{\max}$ is smaller, and this fraction decreases further at 247 nm. In addition, by monitoring the Cl fragments while scanning the photolysis energy we find a broad maximum in the $Cl(^2P_{3/2,1/2})$ yield at 250 nm.

The *ab initio* calculations also show that the vertical electronic transition dipole moment to the $1\,^2A_1$ state is significantly larger than that to the $2\,^2A_1(3s)$ Rydberg state, whose vertical maximum lies at 5.54 eV (224 nm). However, the calculations do not take into account the vibrational Franck–Condon factors and thus provide only upper limits. Note that the $2\,^2A_1$ state has a Rydberg character, and therefore is expected to have a planar geometry similar to that of the cation. Thus, its Franck–Condon factors for excitation from ''cold'' CH_2Cl may be more favorable than those for the $1\,^2A_1$ state, and its contribution, especially at the shortest wavelengths that still exhibit a negative β parameter, cannot be ruled out (see below).

2. Parallel transition

$Cl(^2P_{3/2,1/2})$ fragments with large positive values of β are observed at 240–214 nm, and derive mainly from a parallel transition corresponding to an excited state of B_1 symmetry in the C_{2v} point group. Levchenko and Krylov have found that the lowest excited $^2B_1$ state has a vertical excitation energy of 6.28 eV (corresponding to 197 nm excitation) and a large electronic transition dipole moment. This theoretical result agrees well with a previous measurement of the absorption spectrum of CH_2Cl radical that shows a very strong unstructured absorption band centered at 200 nm.[4] Thus, we believe that the assignment of the Cl fragments with positive β to the $2\,^2B_1 \leftarrow 1\,^2B_1$ transition is secure. According to the calculations, this state corresponds to $\pi^*_{CCl} \leftarrow \pi_{CCl}$ excitation, i.e., promotion of a bonding C–Cl π electron to an antibonding π^* orbital, which would lend a repulsive nature to the potential energy surface in the C–Cl coordinate, and is also known to give rise to strong transitions.

The maximum observed value of the β parameter is smaller than the maximum value of 2.0. There can be several possible reasons for a reduction in β other than dissociation that is slower than a rotational period. For a parallel transition, these include simultaneous excitation of parallel and perpendicular transitions, out-of-plane motions during the dissociation, and tangential, in-plane, nuclear motions that lead to ejection of products in a direction that is not parallel to the dissociating bond.[30–33] One or several of these factors may contribute to the reduction in β in CH_2Cl photodissociation.

As mentioned earlier, in the 240–235 nm photolysis region contributions from both parallel and perpendicular transitions are clearly discerned, because the speed distributions of the Cl fragments corresponding to the two excited states are different. We assign the mixed transition in this region to excitations to the $1\,^2A_1$ and the $2\,^2B_1$ upper states. However, at the shorter wavelengths studied here, the allowed transition to the $2\,^2A_1(3s)$ state can also give rise to products with a negative β. According to the calculations, the electronic transition dipole moment to the $2\,^2A_1$ state is two orders of magnitude smaller than the maximum value for excitation to the $2\,^2B_1$ state,[3] but the $2\,^2B_1 \leftarrow 1\,^2B_1$ absorption cross section in the 240–214 nm wavelength region reported here is more than an order of magnitude smaller than the maximum value.[4] Also, differences in Franck–Condon factors between the transitions are not included in the transition dipole moment calculations. Thus, excitation to the $2\,^2A_1$ state can contribute to the reduction in the measured value of β at the shorter wavelengths. More detailed studies of the product energy and angular distributions in the region 245–210 nm are needed in order to separate the contributions of the possible excited states.

In summary, the main absorption features responsible for the products observed in the 312–214 nm region derive from two valence states, the $1\,^2A_1$ and the $2\,^2B_1$ states, giving rise to a perpendicular and a parallel transition, respectively. Some contribution from the $2\,^2A_1(3s)$ Rydberg state cannot be ruled out.

C. Photodissociation dynamics and product electronic states

Further insight into the dissociation dynamics can be obtained from the internal state distributions of the fragments. In the wavelength region of the $1\,^2A_1 \leftarrow 1\,^2B_1$ transition, $CH_2(\tilde{X}\,^3B_1) + Cl(^2P_{3/2})$ is the main dissociation channel, and $CH_2(\tilde{a}\,^1A_1)$ and $Cl(^2P_{1/2})$ appear only as minor products. In the region of the $2\,^2B_1 \leftarrow 1\,^2B_1$ transition, both $Cl(^2P_{3/2})$ and $Cl(^2P_{1/2})$ are produced in comparable amounts, and they are better correlated with the $CH_2(\tilde{a}\,^1A_1)$ cofragment.

The calculation of the vertical energies of the electronic states allows us to compare our observations to a diabatic state correlation diagram, as shown in Fig. 9. Several points are noteworthy regarding this diagram. First, it does not take into account possible curve crossings along the dissociation pathways, and therefore should only be used as a reference frame for comparison with the experimentally observed product branching ratios. Second, the order of the states is based on *vertical* excitation energies.[3] If the geometries of the excited states are very different, the order of the adiabatic origins of the states may change. Third, the diagram is constructed only in C_{2v} symmetry. If the symmetry is lowered to C_s due to nonplanarity, avoided crossings would change the correlations. Consequently, the differences between the observations and the predictions based on this diagram can only be used to suggest possible interactions between different states of the radical.

As seen from the diagram, both the ground and the first excited states of CH_2Cl correlate with $CH_2(\tilde{X}\,^3B_1) + Cl(^2P_{3/2})$. This is in good agreement with the experimental results where ground-state products dominate. The parallel transition, which involves the $2\,^2B_1$ state, should give rise

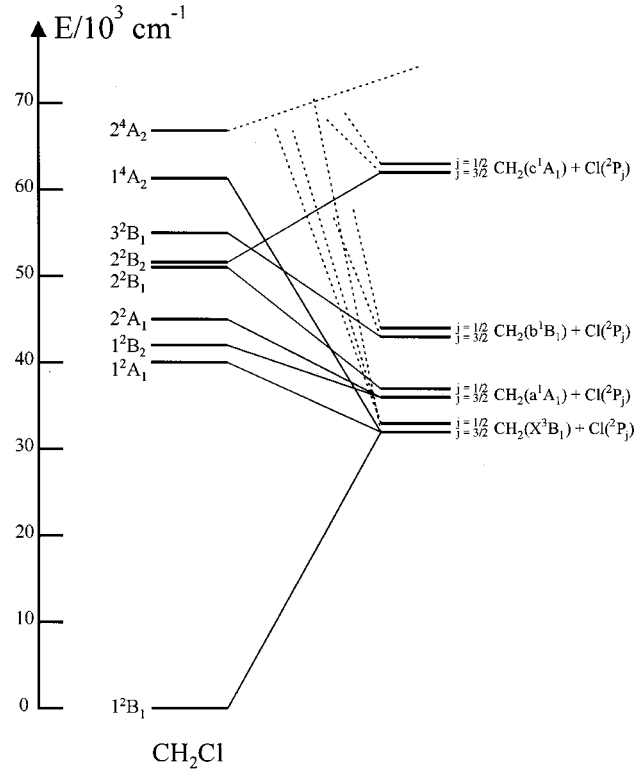

FIG. 9. Diabatic correlation diagram for the dissociation of CH_2Cl to CH_2+Cl. The vertical energies and assignments of the excited electronic states of CH_2Cl are taken from Ref. 3. The excited states energies of CH_2 are taken from Ref. 7.

to $CH_2(\tilde{a}\,^1A_1)$, also in agreement with our interpretation of the experimental Cl energy distributions at 219–214 nm. Significant amounts of Cl fragments correlating energetically with triplet CH_2 are observed only in the region 240–235 nm where the $1\,^2A_1$ and $2\,^2B_1$ states are both excited, and they most likely result from the $1\,^2A_1 \leftarrow 1\,^2B_1$ transition. In the parallel transition, both spin–orbit states or Cl are significantly populated, while according to the correlation diagram $Cl(^2P_{1/2})$ should be preferentially produced. This, however, is not surprising since the Cl spin–orbit states are separated by only 881 cm^{-1}, and long-range exit channel interactions may lead to their mixing.[34]

The agreement in the major features of the observed product branching with a simple diabatic state correlation diagram does not necessarily mean that the products are formed directly from each of these electronic states and that surface crossings are unimportant. The excited radical may experience surface crossings and nonadiabatic interactions along the dissociation pathway that finally converge to the same products predicted ''diabatically.'' A good example is the case of ClO dissociation[35–38] (which is isoelectronic with CH_2Cl), where a bound excited state correlating with $O(^1D)$ products is crossed in the exit channel by several repulsive states, terminating in $O(^3P)$ products.

In order to unravel the dissociation dynamics, more detailed *ab initio* calculations are required. Such calculations must be carried out not only in the vertical excitation region, but also near the equilibrium geometry and in the region of large internuclear separation. Once the adiabatic potential energy surfaces are known, the probabilities of nonadiabatic transitions should be evaluated as well.

Despite the potential complications in interpreting the state correlation diagram, it is safe to suggest that the two electronic states examined in this study give rise to direct dissociation dynamics. The $1\,^2A_1$ state involves promotion of an electron from the singly occupied π^*_{CCl} orbital to an antibonding σ^*_{CCl} orbital, which should weaken and lengthen the C–Cl bond and give rise to repulsion in this coordinate. This is evidenced by the large kinetic energy release in the products, especially at wavelengths where ''cold'' reactants are preferentially excited (e.g., 247 nm). In experiments with Ar, where the final Cl product energy distributions are not as broadened by the rovibrational distribution of the parent CH_2Cl radical, we observe a large narrowing of the first, high-energy, peak (Fig. 5). With Ar, most of the Cl products produced at 266 and 247 nm have translational energies close to the maximum allowed by the energetics. This large kinetic energy release points toward a direct dissociation mechanism taking place on the electronically excited state at these wavelengths.

As discussed above, the parallel transition must also be repulsive in the C–Cl coordinate, as confirmed by the absorption spectrum which is unstructured. For this transition, photodissociation partitions significant fraction of the energy in internal excitation of the $CH_2(\tilde{a}\,^1A_1)$ product. This must reflect either specific motions along the dissociation coordinate, or geometrical differences between the CH_2 moiety in the $2\,^2B_1$ state of CH_2Cl and the free $CH_2(\tilde{a}\,^1A_1)$ radical.

V. SUMMARY

Based on our experimental data and the *ab initio* calculations presented in the accompanying paper, the following conclusions regarding the photochemistry of the CH_2Cl radical at 312–214 nm can be reached.

(1) CH_2Cl generated in a molecular beam via pulsed pyrolysis exhibits continuous, unstructured absorption throughout the investigated region, giving rise to Cl atoms as major products.

(2) The lowest electronically excited state is assigned as $1\,^2A_1$ in C_{2v} symmetry, and is reached via a perpendicular transition. Dissociation occurs on the repulsive part of the potential energy surface terminating in $CH_2(\tilde{X}\,^3B_1) + Cl(^2P_{3/2})$ as a major channel. The equilibrium geometry of the excited state must be very different from that of the ground state; in particular, the C–Cl bond length is different. ''Hot band'' absorption is particularly strong at wavelengths >260 nm. The products are born with substantial translational energy.

(3) The strongest transition is assigned as the $2\,^2B_1 \leftarrow 1\,^2B_1$ parallel transition, and the upper state is repulsive. This transition begins to dominate at $\sim$240 nm, and the absorption cross section increases towards 200 nm. The major products are $CH_2(\tilde{a}\,^1A_1)+Cl(^2P_{1/2,3/2})$, and $CH_2(\tilde{a}\,^1A_1)$ is produced with broad internal excitation. ''Hot band'' absorption is much less important for this transition, indicating a smaller difference in geometry between the ground and $2\,^2B_1$ states.

TABLE I. Calculated rotational energies for selected (N,K) levels of the two photon transition to the $3p$ Rydberg state of $CH_2(\tilde{X}\,^3B_1)$.

(N,K)	$\Delta\omega_{rot}/cm^{-1}$	E_{rot}/cm^{-1}
(0,0)	0.0	0
(1,0)	−0.8	15
(2,0)	−2.4	44
(1,1)	−0.3	81
(3,0)	−4.9	89
(2,1)	−2.0	111
(4,0)	−8.1	148
(3,1)	−4.4	155
(4,1)	−7.6	215
(5,0)	−12.1	222
(5,1)	−11.7	289
(2,2)	−0.5	310
(3,2)	−2.9	355
(4,2)	−6.2	414
(5,2)	−10.2	488
(3,3)	−0.6	687
(4,3)	−3.8	746
(5,3)	−7.8	821
(6,3)	−12.7	910
(4,4)	−0.5	1212
(5,4)	−4.5	1286
(6,4)	−9.4	1375
(5,5)	−0.2	1884
(6,5)	−5.1	1973

The participation of the $2\,^2A_1(3s)$ state in the dissociation is not yet clear, as is the role of possible surface crossings. More theoretical work on the ground and excited state potential energy surfaces is clearly needed. On the experimental front, a search of other dissociation channels is now in progress.

ACKNOWLEDGMENTS

Support by the National Science Foundation and the Donors of the Petroleum Research Fund, administered by the American Chemical Society is gratefully acknowledged. The authors benefited greatly from discussions with Anna Krylov, Sergei Levchenko, and Pavel Jungwirth.

APPENDIX: REMPI SPECTROSCOPY OF THE $CH_2(\tilde{X}\,^3B_1)$ RADICAL

In order to calculate the positions of the rotational lines of $CH_2(\tilde{X}\,^3B_1)$ it is necessary to know the rotational constants for the ground and excited electronic states of the radical. For the ground $^3B_1$ state, the rotational constants are[39] $A''=73.811\,cm^{-1}$, $B''=8.45\,cm^{-1}$, $C''=7.184\,cm^{-1}$. The rotational constants for the excited $3p$-Rydberg state of CH_2 are not known. However, since the geometry of this state is expected to be close to that of the ground state of the cation CH_2^+, the rotational constants for the $3p$-Rydberg state can be evaluated using the same geometry. Geometry optimization was performed with the Q-Chem program package[40] using the DFT method with B3LYP functionals[41] in a 6-311 (+,+)G(3df,3pd) basis set.[42,43] The values obtained [r(CH) $=1.097$ Å, HCH angle$=141.36°$] agree well with previous calculations.[44] The corresponding rotational constants are $A'=73.883\,cm^{-1}$, $B'=7.783\,cm^{-1}$, $C'=7.042\,cm^{-1}$.

Since CH_2 is a near-prolate top in both the ground and the $3p$-Rydberg states, the energy levels for a prolate top are used in the calculations of the rotational energies with $B_{avg}=0.5(B+C)$. The rotational selection rules for a two-photon transition are: $\Delta N=0,\pm1,\pm2$; $\Delta K=0,\pm1,\pm2$. If we consider only transitions with $\Delta N=0$, $\Delta K=0$ (^QQ branch), then the rotational contribution to the total rovibronic transition energy is given by

$$\Delta\omega_{rot}=(B'_{avg}-B''_{avg})N(N+1)+[(A'-B'_{avg})-(A''-B''_{avg})]K^2.$$

Table I shows $\Delta\omega_{rot}$ for transitions originating from selected (N, K) levels, along with their rotational energies. Clearly, many rotational levels have $\Delta\omega_{rot}$ within 10 cm^{-1}. Taking into account the fact that the transitions are broadened by intramolecular interactions,[19] we expect simultaneous excitation of these levels with the detection at 311.8 nm.

[1] B. J. Finlayson-Pitts and J. N. Pitts, Jr., *Chemistry of the Upper and Lower Atmosphere: Theory, Experiments, and Applications* (Academic, New York, 2000).
[2] C. Sandorfy, Top. Curr. Chem. **86**, 91 (1979).
[3] S. V. Levchenko and A. I. Krylov, J. Chem. Phys. **115**, 7485 (2001), following paper.
[4] P. B. Roussel, P. D. Lightfoot, F. Caralp, V. Catoire, R. Lesclaux, and W. Forst, J. Chem. Soc., Faraday Trans. **87**, 2367 (1991).
[5] Y. Endo, S. Saito, and E. Hirota, Can. J. Phys. **62**, 1347 (1984).
[6] S. G. Lias, J. E. Bartmess, J. F. Liebman, J. L. Holmes, R. D. Levin, and W. G. Mallard, *Gas-Phase Ion and Neutral Thermochemistry* [J. Phys. Chem. Ref. Data, Suppl. **17**, 1 (1988)].
[7] NIST Chemistry WebBook: NIST Standard Reference Database No. 69 (February 2000 Release); http://webbook.nist.gov/chemistry/
[8] J. J. DeCorpo, D. A. Bafus, and J. L. Franklin, J. Chem. Thermodyn. **3**, 125 (1971).
[9] M. Weissman and S. W. Benson, J. Phys. Chem. **87**, 243 (1983).
[10] E. Tschuikow-Roux and S. Paddison, Int. J. Chem. Kinet. **19**, 15 (1987).
[11] J. L. Holmes and F. P. Lossing, J. Am. Chem. Soc. **110**, 7343 (1988).
[12] J. A. Seetula, J. Chem. Soc., Faraday Trans. **92**, 3069 (1996).
[13] J. A. Seetula, Phys. Chem. Chem. Phys. **2**, 3807 (2000).
[14] D. W. Kohn, H. Clauberg, and P. Chen, Rev. Sci. Instrum. **63**, 4003 (1992).
[15] E. Kolodney and A. Amirav, Chem. Phys. **82**, 269 (1983).
[16] Th. Droz-Georget, M. Zyrianov, H. Reisler, and D. Chandler, Chem. Phys. Lett. **276**, 316 (1997).
[17] M. Zyrianov, A. Sanov, Th. Droz-Georget, and H. Reisler, J. Chem. Phys. **110**, 10774 (1999).
[18] C. E. Moore, *Atomic Energy Levels* v.I (NSRDS-NBS, 1971).
[19] K. K. Irikura, R. D. Johnson III, and J. W. Hudgens, J. Phys. Chem. **96**, 6131 (1992).
[20] R. N. Bracewell, *The Fourier Transform and Its Applications* (McGraw-Hill, New York, 1986).
[21] K. Mikhaylichenko, C. Riehn, L. Valachovic, A. Sanov, and C. Wittig, J. Chem. Phys. **105**, 6807 (1996).
[22] M. R. Cameron and S. H. Kable, Rev. Sci. Instrum. **67**, 283 (1996).
[23] A. V. Demyanenko, V. Dribinski, A. B. Potter, and H. Reisler (unpublished).
[24] R. D. Johnson III, J. Chem. Phys. **96**, 4073 (1992).
[25] M. E. Jacox and D. E. Milligan, J. Chem. Phys. **53**, 2688 (1970).
[26] L. Andrews and D. W. Smith, J. Chem. Phys. **53**, 2956 (1970).
[27] F. Temps, H. Gg. Wagner, and M. Wolf, Z. Naturforsch., A: Phys. Sci. **47**, 660 (1992).
[28] (a) H. Koch, H. Jørgen, Aa. Jensen, and P. Jørgensen, J. Chem. Phys. **93**, 3345 (1990); (b) J. F. Stanton and R. J. Bartlett, *ibid.* **98**, 7029 (1993).
[29] The axis system in the C_{2v} notation used here is the one customary in spectroscopy, cf. J. M. Hollas, *High Resolution Spectroscopy* (Wiley, New York, 1998), in which the *x* axis is out-of-plane, and the *z* axis is along the C–Cl bond. Note that in the accompanying paper (Ref. 3), a different axis system, common in *ab initio* calculations, is used in which the *y* axis is out-of-plane. However, a nonstandard table of C_{2v} characters is used in

Ref. 3 in order to keep the spectroscopic assignments the same as those customary in spectroscopy.
[30] C. Jonah, J. Chem. Phys. **55**, 1915 (1971).
[31] S. Yang and R. Bersohn, J. Chem. Phys. **61**, 4400 (1974).
[32] H.-P. Loock, J. Cao, and C. X. W. Qian, Chem. Phys. Lett. **206**, 422 (1993).
[33] A. V. Demyanenko, V. Dribinski, H. Reisler, H. Meyer, and C. X. W. Qian, J. Chem. Phys. **111**, 7383 (1999).
[34] J. Cao, Y. Wang, and C. X. W. Qian, J. Chem. Phys. **103**, 9653 (1995).
[35] H. Floyd Davis and Y. T. Lee, J. Phys. Chem. **100**, 30 (1996).
[36] S. Schmidt, Th. Benter, and R. N. Schindler, Chem. Phys. Lett. **282**, 292 (1998).
[37] I. C. Lane, W. H. Howie, and A. J. Orr-Ewing, Phys. Chem. Chem. Phys. **1**, 3087 (1999).
[38] A. Toniolo, M. Persico, and D. Pitea, J. Chem. Phys. **112**, 2790 (2000).
[39] M. E. Jacox, J. Phys. Chem. Ref. Data, 1 (1994), Monograph No. 3.
[40] J. Kong *et al.*, J. Comput. Chem. **21**, 1532 (2000).
[41] P. J. Stephens, F. J. Devlin, C. F. Chabalowski, and M. J. Frisch, J. Phys. Chem. **98**, 11623 (1994).
[42] M. J. Frisch, J. A. Pople, and J. S. Binkley, J. Phys. Chem. **80**, 3265 (1984).
[43] T. Clark, J. Chandrasekhar, and P. V. R. Schleyer, J. Comput. Chem. **4**, 294 (1983).
[44] P. R. Bunker, Can. J. Phys. **72**, 871 (1994).